ISSN 0023-1584, Kinetics and Catalysis, 2008, Vol. 49, No. 3, pp. 428–434. © MAIK "Nauka/Interperiodica" (Russia), 2008.
Original Russian Text © Z.A. Sabirova, M.M. Danilova, V.I. Zaikovskii, N.A. Kuzin, V.A. Kirillov, T.A. Kriger, V.D. Meshcheryakov, N.A. Rudina, O.F. Brizitskii, L.N. Khrobostov, 2008, published in Kinetika i Kataliz, 2008, Vol. 49, No. 3, pp. 449–456.

Nickel Catalysts Based on Porous Nickel for Methane Steam Reforming

Z. A. Sabirova[a], M. M. Danilova[a], V. I. Zaikovskii[a], N. A. Kuzin[a], V. A. Kirillov[a], T. A. Kriger[a], V. D. Meshcheryakov[a], N. A. Rudina[a], O. F. Brizitskii[b], and L. N. Khrobostov[b]

[a] *Boreskov Institute of Catalysis, Siberian Branch, Russian Academy of Sciences, Novosibirsk, 630090 Russia*
[b] *All-Russia Research Institute of Experimental Physics, Russian Federal Nuclear Center, Sarov, Nizhegorodskaya oblast, 607200 Russia*
e-mail: sabirova@catalysis.nsk.su

Received October 17, 2006

Abstract—The influence of synthesis conditions on the phase composition and texture of porous nickel supports as plates with a magnesium oxide underlayer were investigated by X-ray diffraction, low-temperature nitrogen absorption, and electron microscopy combined with X-ray microanalysis. Nickel catalysts supported on these plates were studied. Thermal treatment of $Mg(NO_3)_2$ in nitrogen yields a magnesium oxide underlayer with a small specific surface area (support I). The replacement of nitrogen with hydrogen leads to a larger surface area (support II). The formation of MgO is accompanied by the incorporation of Ni^{2+} cations from the oxide film into the underlayer. Upon subsequent reduction with hydrogen or under the action of the reaction medium, these cations form fine crystallites of nickel. The supports having an oxide underlayer show a higher activity in methane steam reforming than the initial metallic nickel. Nickel catalysts on supports I and II show similar activities. The activity of the catalysts was stable throughout 50-h-long tests; no carbon deposits were detected by TEM.

DOI: 10.1134/S0023158408030178

One of the most promising ways of producing synthesis gas is by MSR. To carry out the endothermic reaction of methane steam reforming (MSR), intensive heat transfer from an outer source to the reaction zone is required. Therefore, the catalyst must have a high thermal conductivity. It is most promising to use catalysts on metallic supports. There are several works in which MSR was carried out using catalysts on metallic supports [1–4]. Test data for a nickel composite catalyst reinforced with a stainless steel network were reported in [1]. That catalyst was obtained by sintering metallic nickel and supported nickel catalyst powders and a chromium oxide admixture. Ismagilov et al. [2, 3] tested an MSR catalyst composed of porous nickel with an oxide underlayer and supported nickel. A catalyst obtained by supporting nickel oxide onto porous nichrome containing a zirconium oxide underlayer has been patented [4]. A composite MSR catalyst can be obtained by capsulation of lanthanum nickelate particles in a cermet obtained by the hydrothermal oxidation of porous aluminum [5].

Magnesium oxide is often used as a support of nickel catalysts for MSR. It shows high thermal stability, reduces carbonization owing to the basic properties of its surface [6–9], and readily forms solid solutions with nickel oxide due to the similarity of their structure parameters, making it possible to obtain fine nickel crystallites [6, 10].

In this work, we consider the influence of preparation conditions on the phase composition and texture of porous nickel supports with a magnesium oxide catalyst carrier and on the catalytic properties of catalysts obtained on these supports in MSR.

EXPERIMENTAL

Nickel catalysts were prepared on porous nickel (pNi) supports as 1-mm-thick plates obtained by rolling [11]. The supports had a specific surface area of 0.13 m^2/g. The magnesium oxide underlayer (5 wt %) was obtained by impregnating the support with a $Mg(NO_3)_2$ solution followed by drying and calcination at 550°C in flowing N_2 (support I) or H_2 (support II). Nickel was supported using a $Ni(NO_3)_2$ solution followed by drying and calcination at 450°C in an N_2 flow. The catalysts were reduced in flowing H_2 at 750°C. The nickel content of the reduced catalysts was 5–9 wt %.

The specific surface area and the pore radius distribution were determined by means of low-temperature nitrogen absorption at 77 K using an ACAP-2400 Micromeritics precision instrument. For a number of samples, the total pore volume and the pore radius distribution were determined using mercury porosimetry. Particle morphology was examined by scanning electron microscopy (SEM) and transmission electron (TEM) microscopy using REM-100U and JEM-2010 instruments with a lattice resolution of 0.14 nm. The

energy-dispersive X-ray fluorescence microanalysis (EDX) of some samples was done using an EDAX energy-dispersive spectrometer with a Si(Li) detector with an energy resolution of 130 eV.

Phase analysis was done using X-ray diffraction patterns obtained on an HZ-4 diffractometer (monochromated CuK_α radiation).

Catalyst activity in the MSR reaction was measured by the circulating flow method under atmospheric pressure at $H_2O/CH_4 = 2$ mol/mol, $T = 750$°C, and an initial mixture flow rate of 11.8 l/h using a stainless steel reactor (volume of 34 cm^3, diameter of 22 mm). The catalysts based on porous nickel were tested as plates ($20 \times 35 \times 1$ mm, 0.7 cm^3) or as a 0.25–0.50 mm size fraction (sample weight of 0.8 g). The commercial catalyst NIAP-18 [12] was tested as a 0.25–0.50 mm size fraction (sample weight of 0.8 g) or as 1/2 of the natural grain (hollow cylinder with an outer diameter of 1.5 cm, an inner diameter of 0.6 cm, a height of 0.48 cm, and a volume of 0.7 cm^3). Before activity measurements, the samples were reduced in an H_2 flow at 750°C for 1 h. Next, hydrogen was replaced with the reaction mixture and measurements were taken after 1 h. The composition of reaction mixtures was determined chromatographically. Catalytic activity measurements for the empty reactor showed that the methane conversion was less than 1%.

RESULTS AND DISCUSSION

Phase Composition and Texture

X-ray diffraction revealed the nickel phase in the metallic supports. In support I, the NiO and MgO phases with a unit cell parameter of 4.206 Å were additionally identified (Table 1). This indicated the formation of a solid solution of NiO in MgO. Furthermore, the sample contained traces of the MgO precursor, apparently magnesium hydroxide nitrate, which showed itself as very weak diffraction peaks. In support II, the Ni and MgO phases with a unit cell parameter of 4.218 A were identified. In the reduced catalysts (750°C, H_2) containing 5.0–8.7 wt % Ni on supports I and II, nickel and a solid solution of NiO in MgO with a unit cell parameter much smaller than that of pure MgO (Table 1) were observed. According to the literature, the unit cell parameter of MgO is 4.211 Å [13] and that of NiO is 4.177 Å [14]. The presence of the $Ni_xMg_{1-x}O$ solid solution after reductive treatment (750°C, H_2) is explained by the fact that the Ni^{2+} cations built in the lattice of the difficult-to-reduce oxide MgO are more resistant to reduction (magnesium is characterized by a higher heat of oxide formation than nickel [15]). The increase in the reduction temperature of NiO upon the formation of the $Ni_xMg_{1-x}O$ solid solution is demonstrated in works [6–10].

Table 1. Unit cell parameters of MgO in the catalysts

Catalyst	a_{MgO}, Å
pNi + 5.0% MgO (I)	4.206
pNi + 5.0% MgO (II)	4.218
5.0% Ni/(pNi + 5.0% MgO) (I)	4.201
7.2% Ni/(pNi + 5.0% MgO) (II)	4.205
8.7% Ni/(pNi + 5.0% MgO) (II)	4.194

The metallic support has a macroporous structure with a small total pore volume: according to mercury porosimetry data, most of the pore volume is due to the pores with a radius of 5 to 30 μm (Fig. 1). The macroporous nature of the support is confirmed by SEM data (Fig. 2): the support has a corpuscular porous structure formed by 3- to 10-μm round crystal blocks intergrown at contact sites.

According to SEM data, magnesium oxide forms a 2- to 3-mm-thick loose and porous layer completely covering the pore walls. In the case of support II, according to low-temperature nitrogen absorption data, the MgO underlayer has fine pores with an average diameter of 40 to 80 Å (Fig. 3). The specific surface

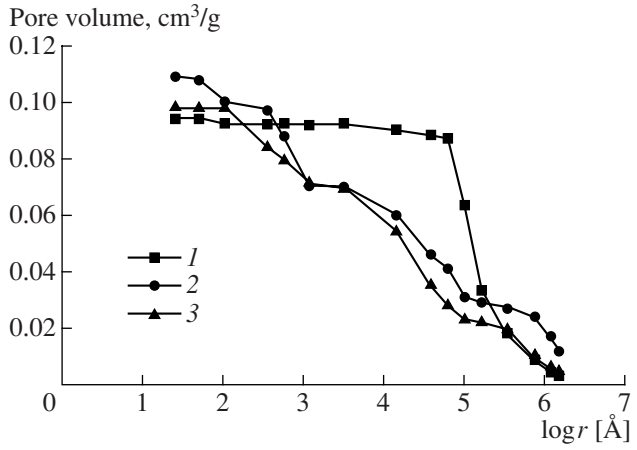

Fig. 1. Pore volume distribution over pore radius: (*1*) pNi, (*2*) pNi + 5.0% MgO (II), and (*3*) 7.2% Ni/(pNi + 5.0% MgO) (II).

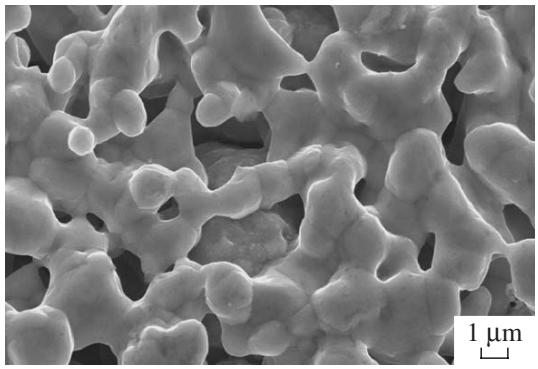

Fig. 2. TEM image of porous nickel metal.

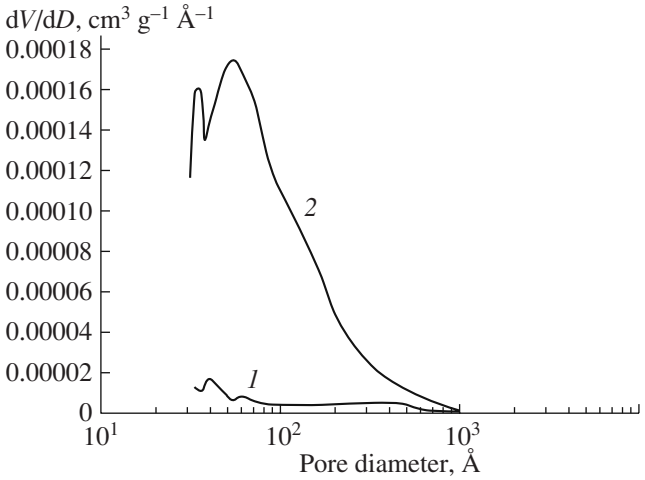

Fig. 3. Pore volume distribution over pore diameter: (*1*) pNi + 5.0% MgO (550°C, N_2) and (*2*) pNi + 5.0% MgO (550°C, H_2).

area of the underlayer is 7.7 m^2/g (Table 2). The replacement of hydrogen with dry nitrogen results in an abrupt decrease in the proportion of fine pores and in the specific surface area down to 0.8 m^2/g (Fig. 3, Table 2). The possible causes of the observed changes in the specific surface area are as follows: firstly the incomplete decomposition of the initial $Mg(NO_3)_2$ in the N_2 flow at a short calcination time [16], as distinct from calcination in flowing hydrogen (a more intensive dehydration of chromium oxide in flowing hydrogen was observed in [17]); secondly, the formation of a surface structure with a higher defect concentration; thirdly, in flowing hydrogen, the amount of water vapor in the pores decreases more sharply and, accordingly, the sintering of MgO particles slows down because of the higher diffusion rate of hydrogen.

Table 2. Texture parameters of the catalysts

Catalyst	S_{sp}, m^2/g	D_{Ni}, Å*
pNi + 5.0% MgO (I)	0.8	–
pNi + 5.0% MgO (I)**	1.2	25–70
pNi + 5.0% MgO (II)	7.7	–
pNi + 5.0% MgO (II)**	7.3	–
5.0% Ni/(pNi + 5.0% MgO) (I)**	2.4	50–100
7.8% Ni/(pNi + 5.0% MgO) (I)**	1.6	50–200
5.7% Ni/(pNi + 5.0% MgO) (II)**	2.7	50–100
7.2% Ni/(pNi + 5.0% MgO) (II)**	–	50–200
8.7% Ni/(pNi + 5.0% MgO) (II)**	2.8	100–200

* The samples were reduced at 750°C in hydrogen.

** Dominant nickel particle size on the MgO surface according to TEM data.

According to TEM data, the MgO underlayer on supports I and II consists of aggregates with a size of 500–1500 Å formed from initial particles 20–70 Å in size. The TEM images of the MgO underlayer (I and II) do not show any separate nickel particles, but only sparse aggregates (~1000 Å), which likely separated from the metallic support during sample preparation. For supports I and II, the EDX spectra of MgO indicate nickel traces (~2 at %) as weak lines (Figs. 4a, 4b). The intensities of the nickel lines in EDX spectra from different MgO areas differ, testifying to different extents of interaction between MgO and NiO from the oxide during heating. It is likely that MgO and NiO particles being in contact interact to yield surface solid solutions or surface compounds [6, 18]. The MgO particles remote from the NiO surface do not react with NiO and do not contain nickel. The general idea of the mechanism of oxide interaction boils down to the cross diffusion of Mg^{2+} and Ni^{2+} cations with oxygen ions remaining fixed. The possibility of interaction between NiO and MgO upon heating in hydrogen at 250–400°C is confirmed by data reported in [18], out of which the authors infer that the diffusion of Ni^{2+} cations to the near-surface layer of MgO occurs simultaneously with their reduction. This also follows from the results reported in [19].

Upon further reduction (750°C, H_2), fine crystallites of nickel (20–70 Å) (Fig. 4c) form on the MgO surface of support I, as is indicated by TEM data; nickel on the MgO surface of support II is still detected only by EDX spectroscopy (Fig. 4d), but nickel crystallites with a size of 20–70 Å appear in the sample tested in the reaction (Fig. 4e). It can be concluded that the fine crystallite of nickel results from the interaction between NiO and MgO. High-resolution TEM shows (Fig. 4e) that the crystallized nickel particles are covered with an oxide layer ~2 nm in thickness. The interplanar spacing in the oxide layer (0.21 nm) is in good agreement with the [002] interplanar spacing in the face-centered structure of nickel oxide [14]. It should be noted that, as a result of reduction with H_2 at 750°C, the MgO agglomerates (support II) are enriched with nickel (Fig. 4d).

The specific surface area of the reduced catalyst and the nickel particle size for supports I and II are similar (Table 2). The similarity of the texture parameters of the nickel catalysts on supports I and II is seemingly due to the rehydration of a considerable part of the magnesium oxide upon impregnation with aqueous $Ni(NO_3)_2$ [20–22]. As the impregnated catalysts are heated to 450°C in flowing nitrogen and from 450 to 750°C in flowing hydrogen, a porous structure more similar in parameters to the initial supports I and II forms there (Table 2).

TEM data (Fig. 5) indicate the epitaxial growth of nickel on the MgO surface [23]: the [111] face of MgO stabilizes the [111] face of Ni. The images of the nickel particles in contact with MgO show a moiré fringe pat-

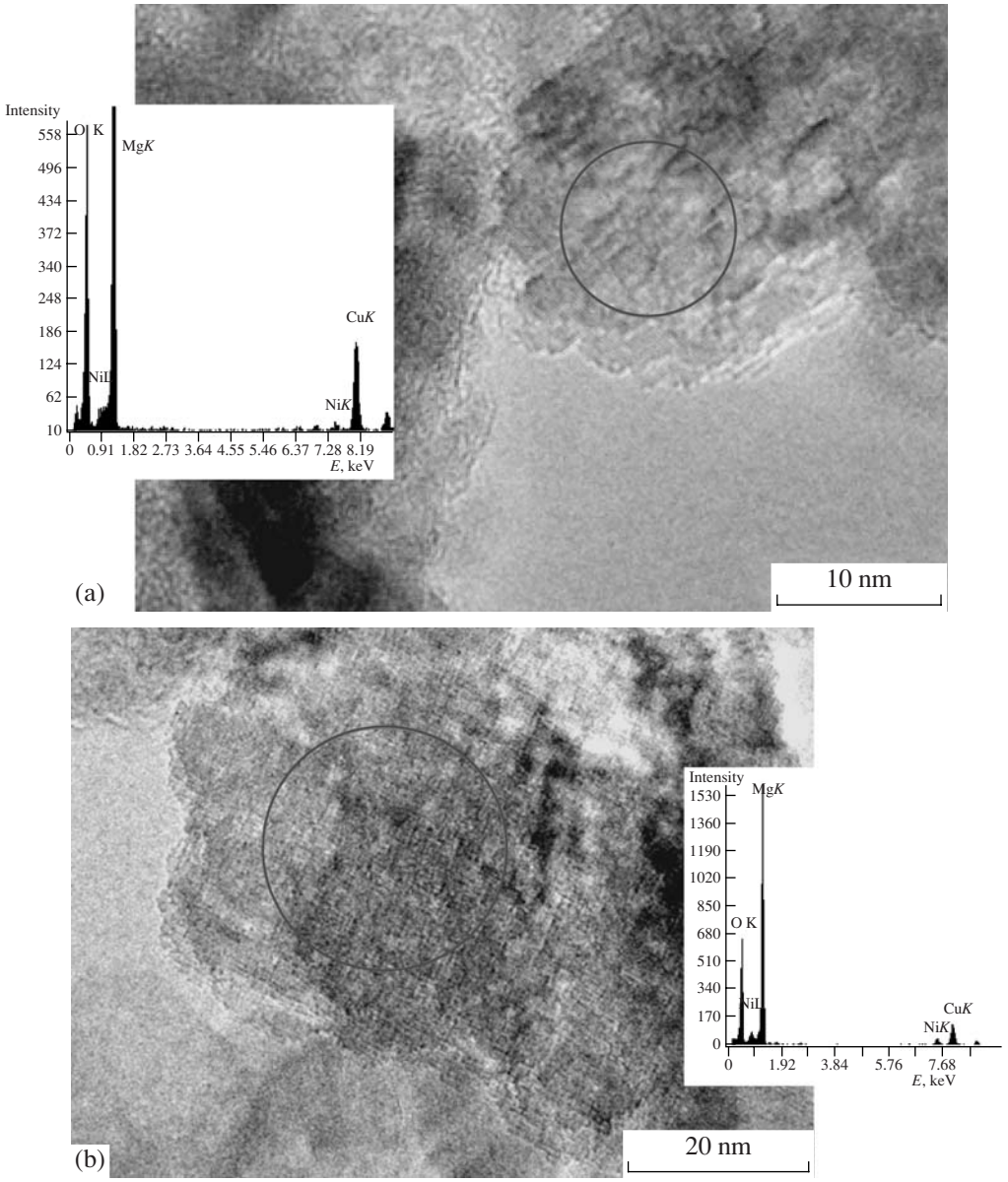

Fig. 4 TEM images of the MgO underlayer on supports (a) I and (b) II obtained by $Mg(NO_3)_2$ decomposition at 550°C in flowing (a) N_2 and (b) H_2; (c) support I after additional reduction at 750°C in H_2; (d) support II after additional reduction at 750°C in H_2; (e) support II after testing in the MSR reaction.

tern [24]. Crystal faces were indexed using interplanar spacing data obtained by high resolution TEM.

Catalytic Activity

Table 3 contains methane conversion data for granular nickel catalysts. The conversion value for the initial nickel support is 20% and increases to 52 and 65% upon the introduction of the MgO (I) and MgO (II) underlayers, respectively. The growth of conversion upon MgO introduction is evidently due to the interaction between NiO and MgO yielding solid solutions, which yield fine nickel crystallites under the action of hydrogen or the reaction medium. The higher activity of the MgO-containing sample obtained by calcination in hydrogen is possibly due to the smaller size of the nickel crystallites forming from the reduction-resistant surface compounds under the action of the reaction medium and to the higher nickel content (Fig. 4d). Additional supporting of nickel raises the methane conversion. The nickel catalysts on supports I and II afford comparable conversions because of the similar average sizes of the supported nickel particles. As the nickel content is increased from 5 to 8–9 wt %, the activity of the catalyst increases slightly (Table 3) because of the coarsening of the nickel particles and the slowdown of the growth of the catalyst surface area per unit weight of the catalyst.

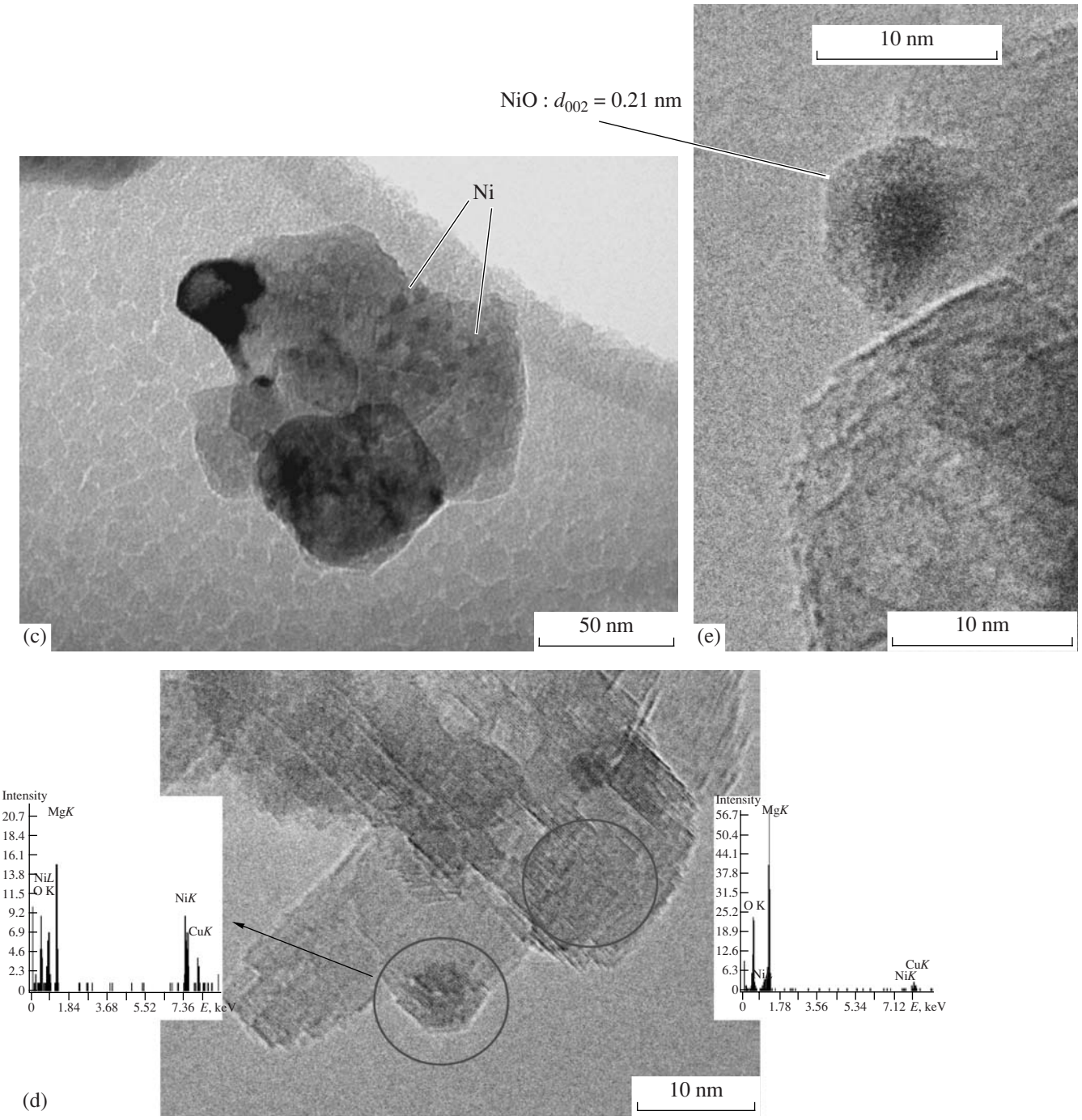

Fig. 4. (Contd.)

According to TEM data, the supported catalysts tested in MSR contain fine nickel crystallites (~20 Å); according to X-ray diffraction data, they do not contain the solid solution phase. It is likely that, under the action of the reaction medium, the reduction of nickel oxide from the reduction-resistant solid solution yielding fine-grained nickel takes place in the supported catalysts.

In this case, NiO is reduced not by dihydrogen, but by H atoms forming in the reaction. Additional heat treatment of the supported catalyst at 550°C in flowing argon for 2 h after an MSR test leads to the partial oxidation of the nickel crystallites and to a decrease in the proportion of crystallites being in epitaxial contact with the MgO underlayer (Fig. 6a). The epitaxial interaction of nickel with the underlayer occurs mainly in the case of the finest Ni particles 20–50 Å in size. When in contact with the underlayer, small particles may flatten. According to electronic microscopy data, a polycrystal-

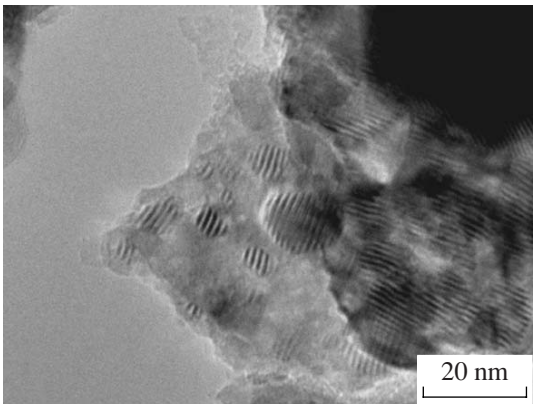

Fig. 5. TEM image of the supported catalyst 5.0% Ni/(pNi + 5.0% MgO) (I).

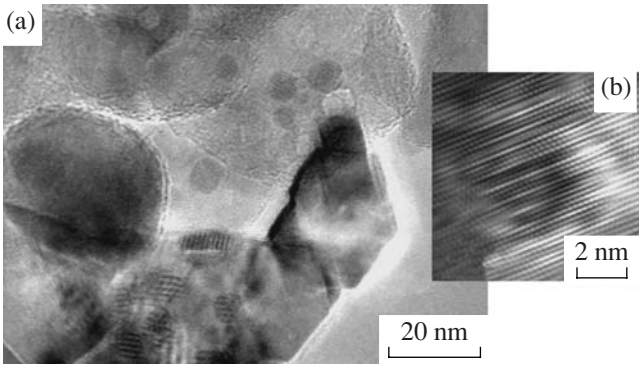

Fig. 6. TEM image of the supported catalyst 5.7% Ni/(pNi + 5.0% MgO) (II) tested in the MSR reaction and additionally treated in flowing Ar at 550°C for 2 h: (a) nickel crystallites on the MgO surface; (b) high resolution TEM image of a fine nickel crystallite having epitaxial contacts with MgO.

line NiO layer ~20 Å in thickness forms on larger nickel crystallites 100–300 Å in size, while the smallest nickel particles (20–50 Å) do not oxidize, and no oxide layer forms on them. Above, we have already mentioned that the presence of nickel oxide is evident from the direct resolution of the lattices planes of the metal and the oxide in the TEM images. Figure 6 shows TEM images (high resolution image in Fig. 6b) demonstrating that all fine nickel crystallites are in the metallic state and contain no oxide layer on their surface. To explain this phenomenon, we assumed that the oxidation of finely divided nickel is suppressed by the interaction of the nickel metal clusters with the MgO surface. It is possible that nickel is oxidized by surface oxygen ions of the underlayer at the metal/oxide interface and, as a consequence, the electron density is shifted towards the underlayer [26]. The cluster has the *Fm*3*m* structure of metallic nickel, but the resulting positive charge ($\delta^+ < 2+$) prevents the oxidation of its outer surface and NiO formation.

Figure 7 shows the dependence of the methane conversion on the duration of the reaction on supported nickel catalysts.

Clearly, the catalysts show stable activity throughout the testing time (50 h). No carbon deposits were observed by TEM in tested samples. It is likely that the hydroxylation of the magnesium oxide surface [27–29] contributes to the coking resistance of the catalysts. Mobile hydroxyl groups migrate to the nickel surface and oxidize the methyl radicals (carbon) forming there [27, 29]. Furthermore, a considerable part of the nickel metal crystallites in the catalysts results from the reduction of the solid solution of NiO in MgO (Table 1) and of surface compounds (Figs. 4a, 4b). It can be assumed that the fine crystallites being formed interact with the underlayer and have catalytic properties different from those of the coarse crystallites. The interaction of the fine nickel particles with the underlayer is confirmed by high-resolution TEM data (Fig. 6b) indicating the absence of the oxide phase in these particles after calcination in argon. An increase of the coking resistance in the case of the solid solution of NiO in MgO being the precursor of the active component was demonstrated in [8, 30, 31]. The stable performance of a nickel catalyst obtained by the reduction of the $Ni_{0.03}Mg_{0.97}O$ solid solution was observed in [8]: at 850°C and H_2O/CH_4 = 1 mol/mol, the activity of the catalyst was invariable throughout the test (65 h). It is suggested that the suppression of coking is due to the interaction between the fine nickel particles resulting from reduction and the oxide underlayer [30]. The influence of the interaction between the catalyst and the support on the coking resistance is also assumed in [32, 33]. Taking into consideration the results reported in [34], one can deduce that, in the catalysts examined, the epitaxial binding of finely divided nickel by the MgO underlayer (Fig. 5) also leads to a change in its catalytic properties and suppresses its activity in the reactions leading to carbon formation.

Table 3. Catalytic activity of the nickel catalysts in MSR

Catalyst	Methane conversion, %	k^*, $cm^3\ (g\ Cat)^{-1}\ atm^{-1}\ s^{-1}$
pNi	20	1.0
pNi + 5.0% MgO (I)	52	4.5
pNi + 5.0% MgO (II)	65	7.7
5.0% Ni/(pNi + 5.0% MgO) (I)	70	9.6
7.8% Ni/(pNi + 5.0% MgO) (I)	72	10.6
5.7% Ni/(pNi + 5.0% MgO) (II)	73	11.1
7.2% Ni/(pNi + 5.0% MgO) (II)	72	10.6
8.7% Ni/(pNi + 5.0% MgO) (II)	76	13.1

* The rate constant of the reaction (k) at 750°C was estimated using a rate equation first-order with respect to methane.

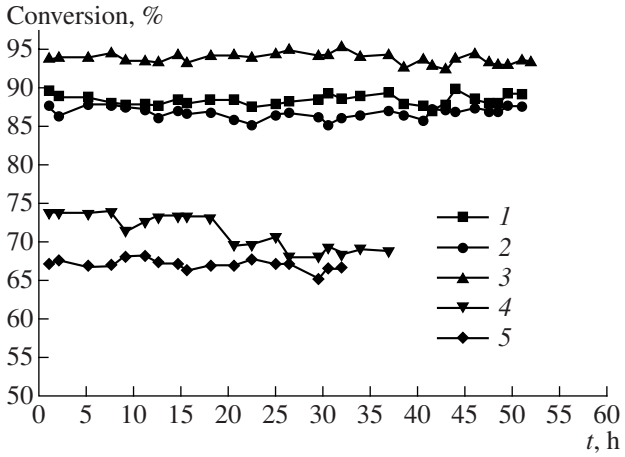

Fig. 7. Methane conversion versus time on stream: (*1*) 5.0% Ni/(pNi + 5.0% MgO) (I) (plate, $V = 0.7$ cm^3, $m = 3.29$ g); (*2*) 5.7% Ni/(pNi + 5.0% MgO) (II) (plate, $V = 0.7$ cm^3, $m = 3.28$ g); (*3*) 7.2% Ni/(pNi + 5.0% MgO) (II) (plate, $V = 0.7$ cm^3, $m = 3.07$ g); (*4*) commercial catalyst NIAP-18 (particle size fraction 0.25–0.50 mm, $m = 0.80$ g); (*5*) commercial catalysts NIAP-18 (1/2 of the natural grain, $V = 0.7$ cm^3, $m = 1.46$ g).

For the catalyst containing 7.2 wt % Ni (plate), the observed methane conversion and the product composition are close to their equilibrium values. A comparison between the nickel catalysts prepared and the commercial catalyst NIAP-18 shows that the activity of the former per unit volume is higher (Fig. 7).

Thus, the nickel catalysts supported on porous nickel plates with a MgO underlayer show stable activities in MSR and are resistant to coking.

ACKNOWLEDGMENTS

The authors are grateful to N.F. Saputina and T.Ya. Efimenko for their assistance.

REFERENCES

1. Kirillov, V.A., Kuzin, N.A., Kulikov, A.V., Fadeev, S.I., Shigarov, A.B., and Sobyanin, V.A., *Teor. Osn. Khim. Tekhnol.*, 2003, vol. 37, no. 3, p. 300 [*Theor. Found. Chem. Eng.* (Engl. Transl.), vol. 37, no. 3, p. 276].
2. Ismagilov, Z.R., Podyacheva, O.Yu., Pushkarev, V.V., et al., *Stud. Surf. Sci. Catal.*, 2000, vol. 130, p. 2759.
3. Ismagilov, Z.R., Pushkarev, V.V., Podyacheva, O.Yu., et al., *Chem. Eng. J.*, 2001, vol. 82, p. 355.
4. Tonkovich, A.L., Yang, B., Perry, S.T., Fitzgerald, S.P., and Wang, Y., *Catal. Today*, 2007, vol. 120, p. 21.
5. Potapova, Yu.V., *Cand. Sci. (Chem.) Dissertation*, Novosibirsk: Boreskov Inst. of Catalysis, 2002.
6. Hu, Y.H. and Ruckenstein, E., *Catal. Rev.*, 2002, vol. 44, no. 3, p. 423.
7. Hu, Y.H. and Ruckenstein, E., *Catal. Lett.*, 1996, vol. 36, p. 145.
8. Yamazaki, O., Tomishige, K., and Fujimoto, K., *Appl. Catal., A*, 1996, vol. 136, p. 49.
9. Parmaliana, A., Arena, F., and Frusteri, F., *J. Catal.*, 1993, vol. 141, p. 34.
10. Yoshida, T., Tanaka, T., and Yoshida, H., *J. Phys. Chem.*, 1996, vol. 100, p. 2302.
11. Tikhonov, G.F., Pyryalov, L.A., and Sorokin, V.K., *Poroshk. Metall.*, 1973, vol. 12, p. 85.
12. Yagodkin, V.I., Fedyukin, Yu.T., Men'shov, V.N., and Daut, V.A., *Khim. Prom–st.*, 2001, vol. 2, p. 7.
13. JCPDS Data File 45-0946.
14. JCPDS Data File 47-1049.
15. *Spravochnik khimika* (Chemist's Handbook), Nikol'skii, B.P., Grigorov, O.N., Pozina, M.E., et al., Eds., Leningrad: Khimiya, 1971, vol. 1, p. 786.
16. Dzis'ko, V.A., Tarasova, D.V., and Karnaukhov, A.P., *Fiziko-khimicheskie osnovy sinteza okisnykh katalizatorov* (Physicochemical Foundations of the Synthesis of Oxide Catalysts), Novosibirsk: Nauka, 1978.
17. Rode, T.V., *Kislorodnye soedineniya khroma i khromovye katalizatory* (Oxygen-Containing Chromium Compounds and Chromium Catalysts), Moscow: Akad. Nauk SSSR, 1962.
18. Bond, G.C. and Sarsam, S.P., *Appl. Catal., A*, 1988, vol. 38, p. 365.
19. Takezawa, N., Terunuma, H., and Shimokawabe, M., Kobayashi, *Appl. Catal.*, 1986, vol. 23, p. 291.
20. Hillerová, E., Vít, Z., and Zdražil, M., *Appl. Catal.*, *A*, 1994, vol. 118, p. 111.
21. Aramendía, M.A., Borau, V., and Jiménez, C., *Appl. Catal.*, 2003, vol. 244, p. 207.
22. Plyasova, L.M., Vasil'eva, N.A., Kriger, T.A., Shmakov, A.N., and Litvak, G.S., *Kinet. Katal.*, 2000, vol. 41, p. 612 [*Kinet. Catal.* (Engl. Transl.), vol. 41, p. 557].
23. Svedberg, E.B., Sandstrom, P., Sundgren, J.-E., Greene, J.E., and Madsen, L.D., *Surf. Sci.*, 1999, vol. 429, p. 206,
24. Hirsch, P.B., Howie, A., Nickolson, R.B., et al., *Electron Microscopy of Thin Crystals*, London: Butterworths, 1965, p. 169.
25. Sobyanin, V.A., Bobrova, I.I., Titova, E.Yu., et al., *React. Kinet. Catal. Lett.*, 1989, vol. 39, no. 2, p. 443.
26. Kuz'minskii, M.B. and Bagatur'yants, A.A., *Itogi Nauki Tekh., Ser.: Kinet. Katal.*, 1980, vol. 8, p. 99.
27. Wei, J. and Iglesia, E., *J. Catal.*, 2004, vol. 224, p. 370.
28. Polychronopoulou, K., Costa, C.N., and Efstathiou, A.M., *Catal. Today*, 2006, vol. 112, p. 89.
29. Aparicio, Z.M., *J. Catal.*, 1997, vol. 165, p. 262.
30. Tomishige, K., Yamazaki, O., Chen, Y., et al., *Catal. Today*, 1998, vol. 45, p. 35.
31. Chen, Y., Tomishige, K., Yokoyama, K., and Fujimoto, K., *J. Catal.*, 1999, vol. 184, p. 479.
32. Khasin, A.A., Yur'eva, T.M., Kaichev, V.V., Zaikovskii, V.I., Demeshkina, M.P., Minyukova, T.P., Baronskaya, N.A., Bukhtiyarov, V.I., and Parmon, V.N., *Kinet. Katal.*, 2006, vol. 47, no. 3, p. 420 [*Kinet. Catal.* (Engl. Transl.), vol. 47, no. 3, p. 412].
33. Khasin, A.A. and Kovalenko, A.S., *Dokl. Akad. Nauk*, 2004, vol. 397, no. 6, p. 786 [*Dokl. Phys. Chem.* (Engl. Transl.), vol. 397, no. 6, p. 194].
34. Kaul, A.R., Gorbenko, O.Yu., and Kamenev, A.A., *Usp. Khim.*, 2004, vol. 73, no. 9, p. 932.